Multistability and self-organization in disordered SQUID metamaterials

2013 Supercond. Sci. Technol. 26 084006

(http://iopscience.iop.org/0953-2048/26/8/084006)

Supercond. Sci. Technol. **26** (2013) 084006 (12pp) doi:10.1088/0953-2048/26/8/084006

Multistability and self-organization in disordered SQUID metamaterials

N Lazarides and G P Tsironis

Department of Physics, University of Crete, PO Box 2208, 71003 Heraklion, Greece
Institute of Electronic Structure and Laser, Foundation for Research and Technology-Hellas, PO Box 1527, 71110 Heraklion, Greece

E-mail: nl@physics.uoc.gr and gts@physics.uoc.gr

Received 27 February 2013, in final form 17 June 2013
Published 11 July 2013
Online at stacks.iop.org/SUST/26/084006

Abstract
Planar arrays of magnetoinductively coupled rf SQUIDs (Superconducting QUantum Interference Devices) belong to the emergent class of superconducting metamaterials that encompass the Josephson effect. These SQUID-based metamaterials acquire their electromagnetic properties from the resonant characteristics of their constitutive elements, i.e., the individual rf SQUIDs. In its simplest version, an rf SQUID consists of a superconducting ring interrupted by a Josephson junction. We investigate numerically the response of a two-dimensional rf SQUID metamaterial with respect to the driving frequency of an externally applied alternating magnetic field in the presence of disorder arising from critical current fluctuations of the Josephson elements; in effect, the resonance frequencies of individual SQUIDs are distributed randomly around a mean value. Bistability is observed in the current amplitude–frequency curves both in ordered and disordered SQUID metamaterials; moreover, bistability is favored by disorder through the improvement of synchronization between SQUID oscillators. Relatively weak disorder widens significantly the bistability region by helping the system to self-organize and leads to nearly homogeneous states that change smoothly with varying driving frequency. Also, the total current of the metamaterial is enhanced, compared with that of uncoupled SQUIDs, through the synergetic action of coupling and synchronization. The existence of simultaneously stable states that provide either high or low total current, allows the metamaterial to exhibit different magnetic responses that correspond to different values of the effective magnetic permeability. At low power of the incident field, high current amplitude states exhibit extreme diamagnetic properties corresponding to negative magnetic permeability in a narrow frequency interval.

(Some figures may appear in colour only in the online journal)

1. Introduction

Advances in theory and nanofabrication techniques have opened many opportunities for researchers to create artificially structured, composite media that exhibit extraordinary properties. The *metamaterials* (MMs) are perhaps the most representative class of materials of this type, exhibiting, among other fascinating properties, negative refractive indices and optical magnetism [1–3]. High-frequency magnetism, in particular, exhibited by the *magnetic metamaterials*, is considered one of the 'forbidden fruits' in the Tree of Knowledge that has been brought forth by metamaterial research [4]. The unique properties of MMs are particularly well suited for novel devices such as hyperlenses, which surpass the diffraction limit [5], and optical cloaks of invisibility [6]. Furthermore, they can form a material base for other functional devices with tuning and switching capabilities [4, 7]. The key element for the construction of MMs has customarily been the split-ring resonator (SRR), a subwavelength 'particle' that is effectively a kind of an artificial 'magnetic atom' [8]. In its simplest version it is just a highly conducting ring with a slit and can be regarded as an inductive–capacitive resonant oscillator. SRRs become nonlinear and therefore tunable with the insertion

of an electronic component (e.g., a diode) in their slits [9]. However, metallic SRRs suffer from high Ohmic losses that place a strict limit on the performance of SRR-based metamaterials, either in the linear or the nonlinear regime, and hamper their use in novel devices. The incorporation of active constituents in metamaterials that provide gain through external energy sources has been recognized as a promising technique for compensating losses [10]. On the other hand, the replacement of the metallic elements with superconducting elements provides both loss reduction and wideband tunability [11]; the latter because of the extreme sensitivity of the superconducting state to external stimuli [7, 11]. Tunability of superconducting metamaterial properties by varying the temperature or an externally applied magnetic field have been recently demonstrated [12–16].

Going a step beyond, the metallic metamaterial elements can be replaced by rf SQUIDs (rf Superconducting QUantum Interference Devices), thus creating SQUID-based metamaterials [17, 18]. The rf SQUID, as shown in figure 1(a), consists of a superconducting ring interrupted by a Josephson junction (JJ) and demonstrates both reduced losses and strong nonlinearities due to the Josephson element [19, 20]. It constitutes the direct superconducting analogue of a nonlinear SRR, playing the role of the 'magnetic atom' in superconducting metamaterials in a way similar to that of the SRR for conventional (metallic) metamaterials [17, 21, 22]. The feasibility of using superconducting circuits with JJs as basic elements for the construction of superconducting thin-film metamaterials [23] and the tunability of one- and two-dimensional rf SQUID arrays over a broad frequency band [24, 25] have been recently demonstrated. Nonlinearity and discreteness in SQUID-based metamaterials may also lead to the generation of nonlinear excitations in the form of discrete breathers [18, 21, 22], time-periodic and spatially localized modes that change locally their magnetic response. Numerous types of SQUID have been investigated since its discovery, while it has found several technological applications [26, 27]. Recent advances that led to nano-SQUIDs make possible the fabrication of SQUID metamaterials at the nanoscale [28]. The use of SQUID arrays in dc current sensors [29], filters [30, 31], magnetometers [32], amplifiers [33–35], radiation detectors [36], flux-to-voltage converters [37], compact antennas [38, 39], linear rf low noise amplifiers [40, 41], output amplifiers for rapid single flux quantum (RSFQ) circuits [42, 43], drivers for digital transmitters [44], as well as in RSFQ electronics [45], has been suggested and realized in the past. However, in most of these works the SQUIDs in the arrays were actually directly coupled through conducting paths. The SQUID-based metamaterial suggested in [17] and investigated further in the present work relies on the magnetic coupling of its elements through dipole–dipole forces due to the mutual inductance between SQUIDs.

Moreover, low (sub-kelvin) temperatures provide access to the quantum regime, where rf SQUIDs can be manipulated as flux and phase qubits [46, 47], the basic element for quantum computation. Inductively coupled SQUID flux qubits can be used for the realization of quantum gates [48],

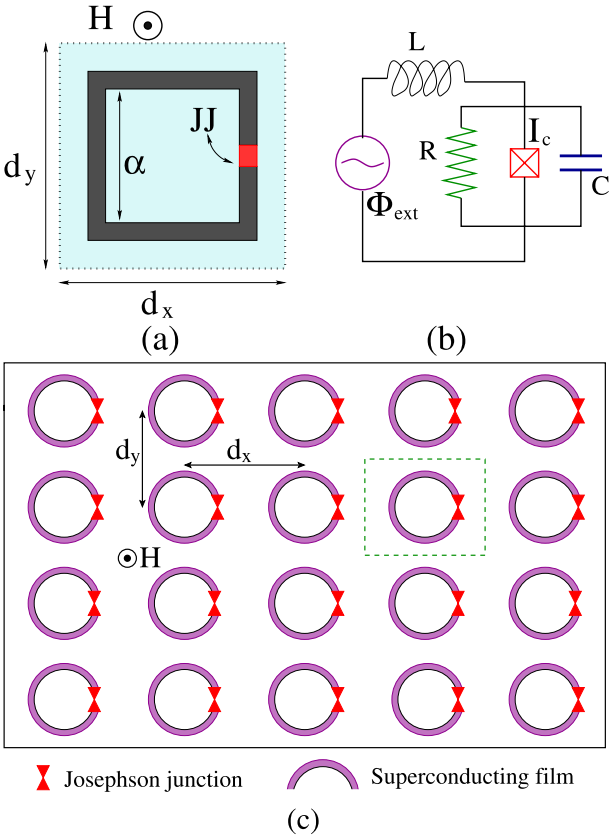

Figure 1. (a) Schematic drawing of an rf SQUID in a perpendicular time-dependent magnetic field $\mathbf{H}(t)$. (b) Equivalent electrical circuit (RCSJ model) for a single rf SQUID driven by a flux source Φ_{ext}. (c) Schematic drawing of a two-dimensional rf SQUID metamaterial, where the unit cell is indicated by the green dashed line.

while larger arrays of inductively coupled SQUID flux qubits have been proposed as scalable systems for adiabatic quantum computing [49, 50]. Notably, amplification and squeezing of quantum noise has been recently achieved with a tunable SQUID-based metamaterial [51]. Other important developments demonstrate clearly that SQUID-based metamaterials enable feedback control of superconducting cubits [52], observation of Casimir effects [53], measurements of nanomechanical motion below the standard quantum limit [54], and three-wave mixing [55].

In the present work we investigate the response of a two-dimensional (2D) rf SQUID metamaterial in the planar geometry with respect to the frequency of an alternating magnetic field, focusing on the effect of quenched disorder. We are particularly interested in frequencies near resonance where multiple responses may appear; this issue is related to the existence or not of a bistability region in the current amplitude–frequency curve of the SQUID metamaterial. Having calculated the response of the metamaterial to a given field, the effective magnetic permeability μ_{r} can be determined by temporal and spatial averaging. Different responses, corresponding to different simultaneously stable metamaterial states, result in different μ_{r} in the bistability region. In the next section we give a brief overview of the equations for a single SQUID, then introduce the equations for

the flux dynamics in a 2D SQUID metamaterial and calculate its linear modes. In section 3 we present numerical results for the current amplitude of the metamaterial as a function of the driving frequency. Such current amplitude–frequency curves are calculated both for ordered and disordered SQUID metamaterials, and reveal the existence of bistability over broad frequency intervals. The disorder is introduced through random variations of the critical currents of the JJs from one SQUID to another due to unavoidable imperfections in fabrication. We thus abandon the assumption of SQUID metamaterials comprising identical elements and allow the critical currents to vary randomly around a target (mean) value. In effect, the natural frequencies of individual SQUIDs are distributed around the value that corresponds to that obtained for the mean critical current. In section 4 we discuss the effect of synchronization and present calculations of the relative magnetic permeability μ_r. Section 5 contains the conclusions.

2. Dynamic equations and linear modes

In an ideal JJ, the current–phase relation is of the form $I = I_c \sin(\phi_j)$, where I_c is the critical current of the JJ and ϕ_j the Josephson phase. When driven by an external magnetic field $H(t)$, the induced (super)currents around the SQUID ring are determined by the celebrated Josephson relations [56]. In the equivalent circuit picture, the resistively and capacitively shunted junction (RCSJ) model is frequently adopted to describe a real JJ. Thus, the equivalent lumped circuit for the rf SQUID in a magnetic field with appropriate polarization comprises a flux source Φ_{ext} in series with an inductance L and an ideal JJ, while the latter is shunted by a capacitor C and a resistor R (figure 1(b)). Then, the dynamic equation for the flux threading the SQUID ring can be obtained by application of Kirchhoff laws, as

$$C\frac{d^2\Phi}{dt^2} + \frac{1}{R}\frac{d\Phi}{dt} + I_c \sin\left(2\pi\frac{\Phi}{\Phi_0}\right) + \frac{\Phi - \Phi_{ext}}{L} = 0, \quad (1)$$

where Φ_{ext} is the external flux, Φ_0 is the magnetic flux quantum, and t is the temporal variable. The flux Φ threading the SQUID ring is related to the Josephson phase through the flux quantization condition

$$\phi_j = 2\pi\frac{\Phi}{\Phi_0} + 2\pi n, \quad (2)$$

where n can be any integer. The rf SQUID is a highly nonlinear oscillator whose amplitude–frequency curves exhibit several peculiar features not seen in conventional inductive–capacitive oscillators. For example, on a fine scale one may observe internal structure whose complexity increases with increasing SQUID parameter β [57], where

$$\beta = \frac{\beta_L}{2\pi}; \qquad \beta_L = 2\pi\frac{LI_c}{\Phi_0}. \quad (3)$$

That fine structure of the amplitude–frequency curves can be reproduced numerically by integrating the dynamic equation (1) [18, 22]. The SQUID resonance can be tuned either by varying the amplitude of the alternating driving field or by varying the magnitude of a static (dc) field threading the SQUID ring that creates a flux bias. The resonance shift due to nonlinearity has actually been observed in a Josephson parametric amplifier driven by fields of different power levels [35], while the shift with applied dc flux has been seen in high-T_c rf SQUIDs [58] and very recently in a low-T_c rf SQUID in the linear regime [23]. Systematic measurements on microwave resonators comprising SQUID arrays have been presented [35, 59]. For very low amplitudes of the driving field (linear regime), the rf SQUID exhibits a resonant magnetic response at a particular frequency

$$\omega_{SQ} = \omega_0\sqrt{1+\beta_L}, \quad (4)$$

where

$$\omega_0 = \frac{1}{\sqrt{LC}}, \quad (5)$$

is the inductive–capacitive (LC) SQUID frequency. The dynamic behavior of the rf SQUID has been studied extensively for more than two decades both in the hysteretic ($\beta_L > 1$) and the non-hysteretic regimes, usually under an external flux field of the form

$$\Phi_{ext} = \Phi_{dc} + \Phi_{ac}\cos(\omega t), \quad (6)$$

where ω is the driving frequency. The first and second term on the right-hand-side of the earlier equation correspond to the fluxes due to the presence of a constant (dc) and an alternating (ac) spatially uniform magnetic field, respectively. Equation (1) is formally equivalent to that of a massive particle in a tilted washboard potential

$$U_{SQ} = \frac{1}{C}\left\{\frac{(\Phi - \Phi_{ext})^2}{2L} - E_J\cos\left(2\pi\frac{\Phi}{\Phi_0}\right)\right\}, \quad (7)$$

with $E_J = I_c\Phi_0/(2\pi)$ being the Josephson energy. The potential (7) has a number of minima that depends on the value of β_L, while their location varies with an applied dc flux. For $\beta_L < 1$ the potential has a single minimum, which moves to the right with increasing dc flux Φ_{dc}, as shown in figure 2(a). For $\beta_L > 1$ there is more than one minimum, with the number increasing on further increasing β_L. An applied dc flux Φ_{dc} can move these minima as well (figure 2(b)). The emergence of more and more minima with increasing β_L at zero dc flux is illustrated in figure 2(c).

Consider a planar array comprising identical rf SQUIDs arranged in a tetragonal $N_x \times N_y$ lattice, that is placed in a spatially uniform, alternating magnetic field directed perpendicularly to the plane of the SQUIDs. A schematic drawing of the array is shown in figure 1(c), where the unit cell is indicated by the green dashed line. The flux threading each SQUID ring induces a current with both normal and superconducting components that generates its own magnetic field. The induced fields couple the SQUIDs to each other through magnetic dipole–dipole interactions. The strength of this magnetoinductive coupling falls off approximately as the inverse-cube of the distance between SQUIDs. If the distance between neighboring SQUIDs is such that they are weakly coupled, then next-nearest and more distant neighbor coupling can be neglected. In that case, we need to take into account

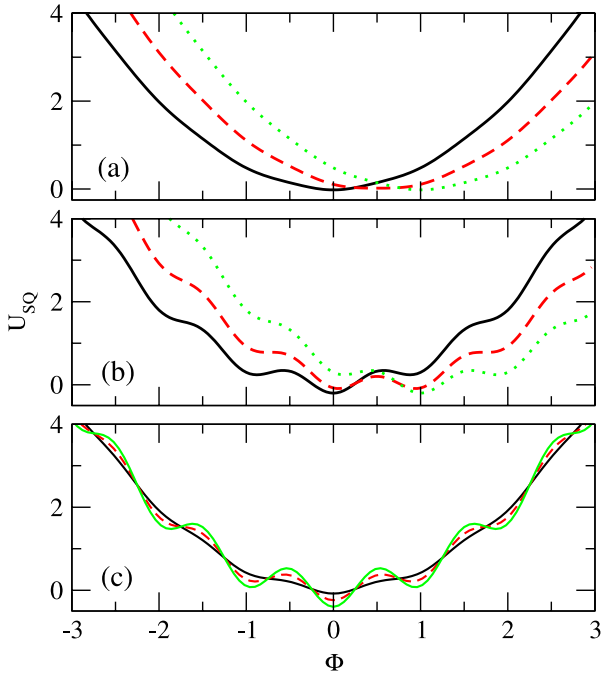

Figure 2. Potential curves as a function of the flux threading the SQUID ring. (a) For a non-hysteretic SQUID with $\beta_L \simeq 0.75 < 1$ and $\phi_{\rm dc} = \Phi_{\rm dc}/\Phi_0 = 0$ (black solid curve); 0.5 (red dashed curve); 1.0 (green dotted curve). (b) For a hysteretic SQUID with $\beta_L \simeq 8 > 1$ and $\phi_{\rm dc} = \Phi_{\rm dc}/\Phi_0 = 0$ (black solid curve); 0.5 (red dashed curve); 1.0 (green dotted curve). (c) For $\Phi_{\rm dc} = 0$ and $\beta_L = 0.5 < 1$ (black solid curve); 1.5 (red dashed curve); 2.5 (green dotted curve).

only nearest-neighbor interactions, and the flux threading (n, m)th SQUID of the array is given by

$$\Phi_{n,m} = \Phi_{\rm ext} + L[I_{n,m} + \lambda_x(I_{n-1,m} + I_{n+1,m}) + \lambda_y(I_{n,m-1} + I_{n,m+1})], \quad (8)$$

where $n = 1, \ldots, N_x$, $m = 1, \ldots, N_y$, $I_{n,m}$ is the total current induced in the (n, m)th SQUID, and $\lambda_{x,y} \equiv M_{x,y}/L$ are the magnetic coupling constants between neighboring SQUIDs in the x and y directions, respectively. The values of the M_x and M_y are negative since the magnetic field generated by the induced current in a SQUID crosses the neighboring SQUID in the opposite direction. By adopting the RCSJ model, the current $I_{n,m}$ is

$$-I_{n,m} = C\frac{{\rm d}^2\Phi_{n,m}}{{\rm d}t^2} + \frac{1}{R}\frac{{\rm d}\Phi_{n,m}}{{\rm d}t} + I_{\rm c}\sin\left(2\pi\frac{\Phi_{n,m}}{\Phi_0}\right). \quad (9)$$

Then, following the procedure of [18] and neglecting terms of order $\lambda_x\lambda_y$, λ_y^2, λ_x^2, etc, we get

$$LI_{n,m} = \Phi_{n,m} - [1 - 2(\lambda_x + \lambda_y)]\Phi_{\rm ext} - \lambda_x(\Phi_{n-1,m} + \Phi_{n+1,m}) - \lambda_y(\Phi_{n,m-1} + \Phi_{n,m+1}). \quad (10)$$

Combining equations (9) and (10) we have

$$C\frac{{\rm d}^2\Phi_{n,m}}{{\rm d}t^2} + \frac{1}{R}\frac{{\rm d}\Phi_{n,m}}{{\rm d}t} + I_{\rm c}\sin\left(2\pi\frac{\Phi_{n,m}}{\Phi_0}\right) - \lambda_x(\Phi_{n-1,m} + \Phi_{n+1,m}) - \lambda_y(\Phi_{n,m-1} + \Phi_{n,m+1}) = [1 - 2(\lambda_x + \lambda_y)]\Phi_{\rm ext}. \quad (11)$$

In the absence of losses ($\gamma = 0$), the earlier equations can be obtained from the Hamiltonian function

$$H = \sum_{n,m}\frac{Q_{n,m}^2}{2C} + \sum_{n,m}\left[\frac{1}{2L}(\Phi_{n,m} - \Phi_{\rm ext})^2 - E_J\cos\left(2\pi\frac{\Phi_{n,m}}{\Phi_0}\right)\right] - \sum_{n,m}\frac{\lambda_x}{L}(\Phi_{n,m} - \Phi_{\rm ext})(\Phi_{n-1,m} - \Phi_{\rm ext}) - \sum_{n,m}\frac{\lambda_y}{L}(\Phi_{n,m} - \Phi_{\rm ext})(\Phi_{n,m-1} - \Phi_{\rm ext}), \quad (12)$$

where

$$Q_{n,m} = C\frac{{\rm d}\Phi_{n,m}}{{\rm d}t} \quad (13)$$

is the canonical variable conjugate to $\Phi_{n,m}$, and represents the charge accumulating across the capacitance of the JJ of each rf SQUID. The Hamiltonian function (12) is the weak coupling version of that proposed in the context of quantum computation [49]. Using the relations

$$\phi_{n,m} = \frac{\Phi_{n,m}}{\Phi_0}, \qquad \phi_{\rm ext} = \frac{\Phi_{\rm ext}}{\Phi_0}, \qquad \tau = \omega_0 t, \qquad \Omega = \frac{\omega}{\omega_0}, \quad (14)$$

equation (11) can be normalized to

$$\ddot{\phi}_{n,m} + \gamma\dot{\phi}_{n,m} + \phi_{n,m} + \beta\sin(2\pi\phi_{n,m}) - \lambda_x(\phi_{n-1,m} + \phi_{n+1,m}) - \lambda_y(\phi_{n,m-1} + \phi_{n,m+1}) = \phi_{\rm eff}, \quad (15)$$

where the overdots denote differentiation with respect to the normalized time τ. The effective driving field and the loss coefficient of individual SQUIDs are given, respectively, by

$$\phi_{\rm eff} = [1 - 2(\lambda_x + \lambda_y)]\phi_{\rm ext}; \qquad \phi_{\rm ext} = \phi_{\rm dc} + \phi_{\rm ac}\cos(\Omega\tau), \quad (16)$$

and

$$\gamma = \frac{1}{R}\sqrt{\frac{L}{C}}. \quad (17)$$

The coefficient γ actually represents all of the dissipation coupled to each rf SQUID and may also include radiative losses [60].

SQUID metamaterials support magnetoinductive flux waves [18], just like conventional metamaterials comprising metallic elements [61]. The frequency dispersion for small amplitude flux waves is obtained by the substitution of $\phi = A\exp[{\rm i}(\kappa_x n + \kappa_y m - \Omega\tau)]$, into the linearized equation (15) without losses and external field (i.e., $\sin(2\pi\phi_{n,m}) \simeq 2\pi\phi_{n,m}$, $\gamma = 0$, $\phi_{\rm ext} = 0$). Thus we get

$$\Omega \equiv \Omega_{\boldsymbol{\kappa}} = \sqrt{1 + \beta_L - 2(\lambda_x\cos\kappa_x + \lambda_y\cos\kappa_y)}, \quad (18)$$

where $\Omega_{\boldsymbol{\kappa}} = \omega/\omega_0$ is the normalized eigenfrequency and $\boldsymbol{\kappa} = (\kappa_x, \kappa_y)$ is the normalized wavevector. The components of $\boldsymbol{\kappa}$ are related to those of the wavevector in physical units

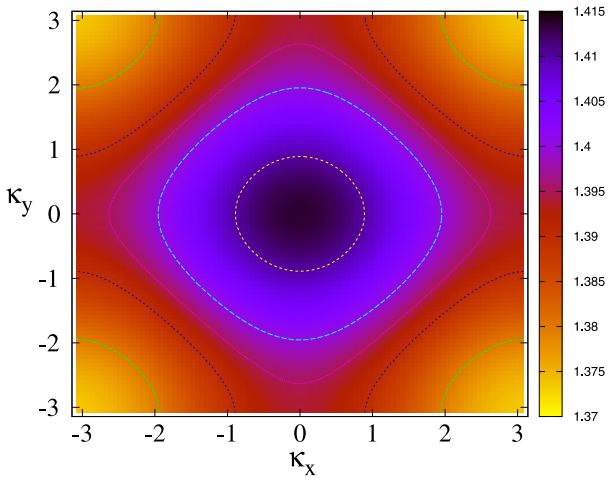

Figure 3. Density plot and contours of the linear dispersion $\Omega_{\mathbf{k}}$ on the κ_x–κ_y plane from equation (18), for a two-dimensional SQUID metamaterial with $\lambda_x = \lambda_y = -0.014$ and $\beta = 0.15$.

$\mathbf{k} = (k_x, k_y)$ through $\kappa_{x,y} = d_{x,y}\, k_{x,y}$, with d_x and d_y being the wavevector component and center-to-center distance between neighboring SQUIDs in the x- and y-directions, respectively. A typical density plot of the dispersion (18) on the κ_x–κ_y plane is shown in figure 3 for a tetragonal (i.e., $d_x = d_y$) SQUID metamaterial.

3. Current–frequency curves

In order to calculate the current amplitude of the SQUID metamaterial as a function of the driving frequency, we integrate equation (15) for the normalized flux values $\phi_{n,m}$. Then, the normalized current in the (n, m)th SQUID, $i_{n,m}$, can be obtained from the normalized version of equation (10) which, after some rearrangement, reads

$$i_{n,m} = \frac{1}{\beta}\{\phi_{n,m} - \phi_{\rm eff} - \lambda_x(\phi_{n-1,m} + \phi_{n+1,m}) - \lambda_y(\phi_{n,m-1} + \phi_{n,m+1})\}, \quad (19)$$

where $\phi_{\rm eff}$ is given by equation (16). For a single SQUID, the (normalized) current amplitude is the absolute maximum current in one period of evolution, which is denoted by $i_{\rm max}$. In the case of ordered SQUID metamaterials we use the same notation for the current amplitude, which in this case is defined as the absolute maximum of the total current $i_{\rm tot}(t) = \sum_{n,m} i_{n,m}(t)$ divided by the number of SQUIDs $N_x N_y$, in one period of evolution, i.e.,

$$i_{\rm max} = \max_T \left\{ \frac{1}{N_x N_y} \sum_{n,m} i_{n,m}(t) \right\}, \quad (20)$$

with $T = 2\pi/\Omega$. The corresponding quantity for disordered SQUID metamaterials is denoted by $\langle i_{\rm max}\rangle$, where the brackets indicate averaging of $i_{\rm max}$ over the number of different realizations, $n_{\rm R}$. In the following, equation (15) is implemented with the boundary conditions (except otherwise stated)

$$\phi_{0,m}(\tau) = \phi_{N_x+1,m}(\tau) = \phi_{n,0}(\tau) = \phi_{n,N_y+1}(\tau) = 0, \quad (21)$$

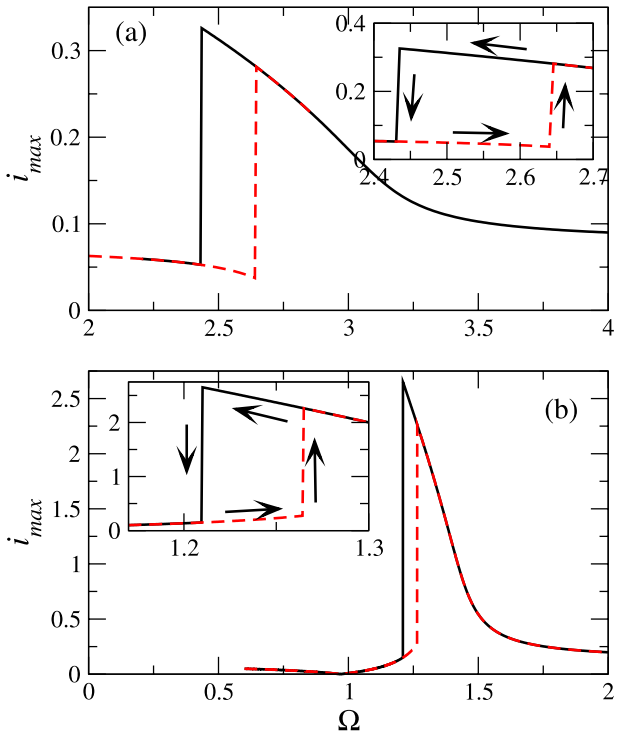

Figure 4. Current amplitude $i_{\rm max}$ as a function of the driving frequency Ω for an rf SQUID with $\alpha = 0.002$, $\phi_{\rm dc} = 0$, and (a) $\beta = 1.27$, $\phi_{\rm ac} = 0.1$; (b) $\beta = 0.15$, $\phi_{\rm ac} = 0.02$. An enlargement of the bistability region is shown in the insets for each case.

which account for the termination of the structure in a finite system. The set of dynamic equations (15) are integrated in time with a standard fourth-order Runge–Kutta algorithm. Note that the normalized resonance frequency for a single rf SQUID, $\Omega_{\rm SQ}$, is given in units of its corresponding LC frequency, i.e., $\Omega_{\rm SQ} = \omega_{\rm SQ}/\omega_0 = \sqrt{1+\beta_L}$ (see equation (4)). Thus, for the values of the SQUID parameters used in the following, i.e., $\beta_L = 1.27$ and $\beta_L = 0.15$, the normalized resonance frequencies are $\Omega_{\rm SQ} \simeq 3.0$ and $\Omega_{\rm SQ} \simeq 1.4$, respectively. Typical current amplitude–frequency curves for a single SQUID are shown in figure 4 (for $\Phi_{\rm dc} = 0$), which exhibit bistability regions that are shown more clearly in the insets. The frequency intervals of high current amplitude, where bistability appears in figures 4(a) and (b), are located below the values of 3.0 and 1.4, respectively, due to nonlinearity [22]. In order to trace the current amplitude–frequency curves for ordered ($i_{\rm max} - \Omega$) or disordered ($\langle i_{\rm max}\rangle - \Omega$) arrays, we start the system with zero initial conditions and start integrating with a low (high) frequency until a steady state is reached. Subsequently the frequency is increased (decreased) by a small amount and the equations are again integrated until a steady state is reached, and so on. In each frequency step (except the first one, where we use zeros) we use as initial condition the steady state solution obtained in the previous step. We assume a moderate size array with $N_x = N_y = 20$, for which the coupling between SQUIDs is isotropic and weak, i.e., $\lambda_x = \lambda_y = -0.014$. Typical current amplitude–frequency curves are shown in figure 5, where the current amplitude $i_{\rm max}$ is

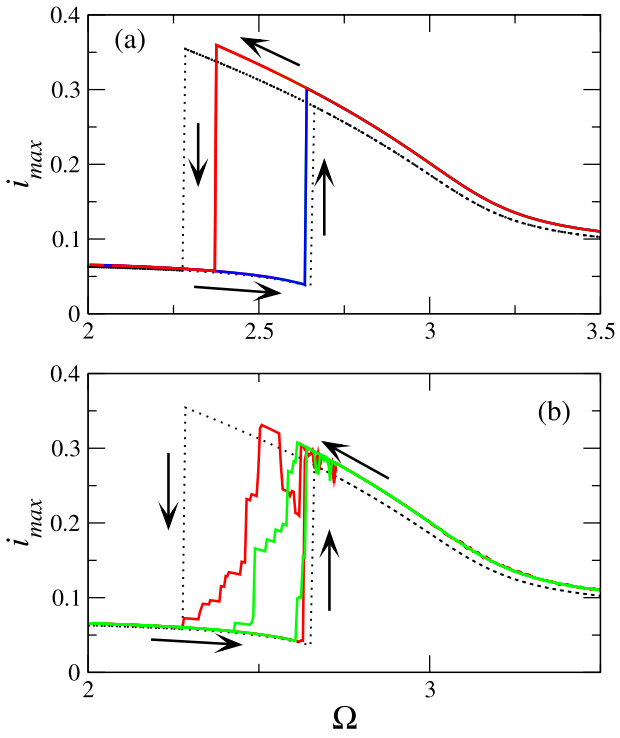

Figure 5. Current amplitude $i_{\max}$ as a function of the driving frequency Ω for two-dimensional $N_x \times N_y$ SQUID metamaterials with $\alpha = 0.002$, $\beta = 1.27$, $\phi_{dc} = 0$, $\phi_{ac} = 0.1$, $N_x = N_y = 20$, and (a) periodic boundary conditions; (b) free-end boundary conditions, starting with different initializations. The black dotted lines indicate the corresponding $i_{\max}$ versus Ω curves for a single rf SQUID.

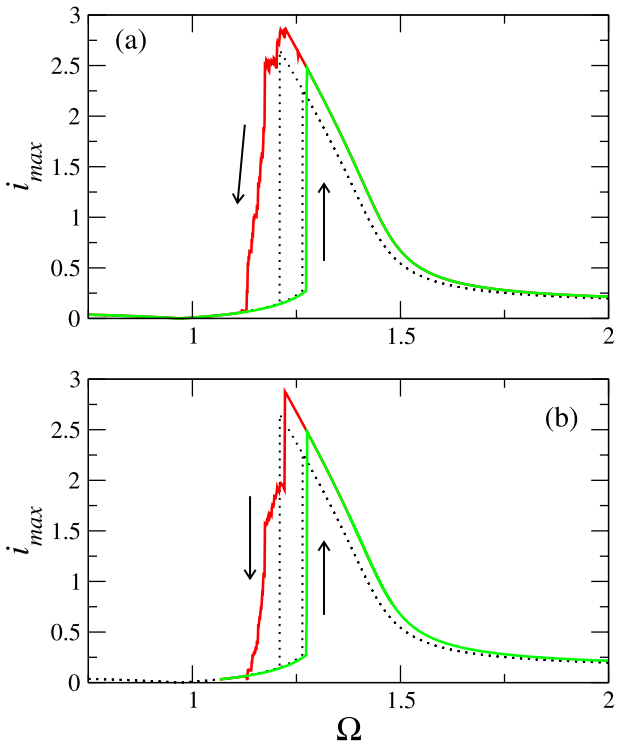

Figure 6. Current amplitude $i_{\max}$ as a function of the driving frequency Ω for two-dimensional $N_x \times N_y$ SQUID metamaterials with $\alpha = 0.002$, $\beta = 0.15$, $\phi_{dc} = 0$, $\phi_{ac} = 0.02$, and (a) $N_x = N_y = 20$; (b) $N_x = N_y = 40$. The black dotted lines indicate the corresponding $i_{\max}$ versus Ω curves for a single rf SQUID. Free-end boundary conditions that account for the termination of the structure have been used.

displayed as function of the frequency Ω of an alternating flux (dc flux is set to zero). In this figure, the value of the parameter β has been selected so that hysteretic effects are rather strong ($\beta_L \simeq 8$). We observe that bistability appears in a frequency region of significant width. The corresponding curves for a single SQUID are also shown for comparison. In figure 5(a), where periodic boundary conditions have been employed, we observe that although the bistability region for the array is narrower than that for a single SQUID, the current amplitude is slightly larger than that for a single SQUID. In the case of periodic boundary conditions, the size of the array does not affect those results; current amplitude–frequency curves for larger arrays with $N_x = N_y = 40$ and $N_x = N_y = 80$ (not shown) are practically identical to those shown in figure 5(a). In figure 5(b) and the rest of the paper, free-end boundary conditions (equations (21)) have been used. In this case, the current amplitude–frequency curves are very sensitive to the initial conditions, the frequency step, and other parameters. The curves in figure 5(b) shown in different colors (red and green) correspond to different initializations of the same system.

The parts of the current amplitude–frequency curves that are close to those for a single SQUID are formed by almost homogeneous states, i.e., states with all SQUIDs in the high current amplitude or low current amplitude state. Homogeneous states are formed more easily in the periodic systems (figure 5(a)); only a small part survives in the case of free-end boundary conditions (figure 5(b)) that is close to the current amplitude–frequency curve of a single SQUID. In the latter figure we also observe the formation of small steps for which the corresponding solutions may be characterized as 'mixed states' that are formed by a certain number of SQUIDs in the high current amplitude state while all the others are in the low current amplitude state. In figure 6, the corresponding curves for SQUIDs with $\beta_L \simeq 1$ ($\beta = 0.15$) are shown. A comparison with the corresponding curves for a single SQUID (shown as dotted black lines) indicates that the frequency regions where bistability appears are nearly of the same width.

Up to this point, we have considered SQUID metamaterials comprising identical units. Next, we take into account imperfections in fabrication leading to non-identical parameters from one SQUID to another; specifically, we allow the critical currents of the Josephson junctions to vary randomly around a mean value. In the normalized form of the equations, the variation of the critical currents affects the SQUID parameters β, which in turn determine the resonance frequency of individual SQUIDs. Although it is not possible to fabricate absolutely identical SQUIDs, the existing experience with dc SQUID arrays shows that the available fabrication technology allows the fabrication of SQUID arrays with nearly identical parameters (within a few per cent). In contrast, when it is necessary to fabricate SQIF arrays, i.e., arrays of non-identical SQUIDs, the degree of their disorder is designed on purpose [62–64]. We have calculated the current amplitude–frequency curves

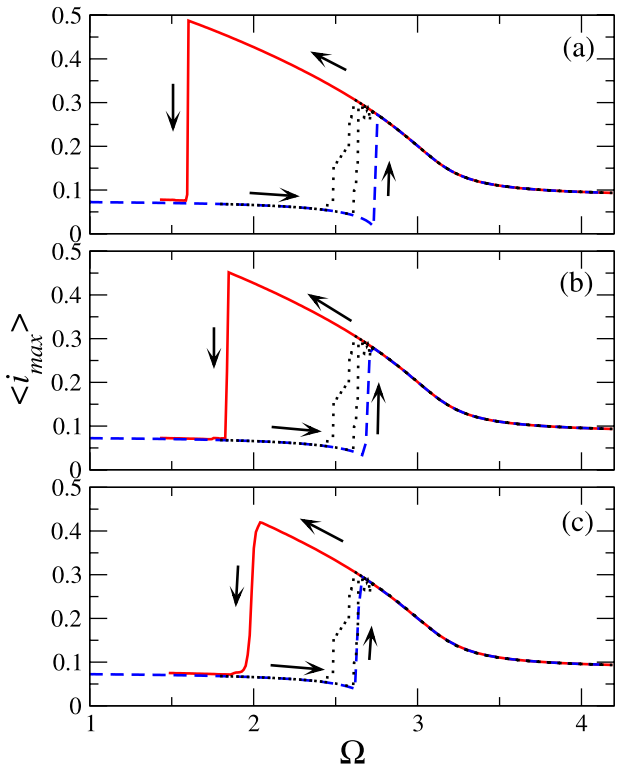

Figure 7. Current amplitude averaged over $n_R = 30$ realizations of disorder, $\langle i_{max} \rangle$, as a function of the driving frequency Ω for a SQUID metamaterial with $\alpha = 0.002$, $\beta = 1.27$, $\phi_{ac} = 0.1$, $\phi_{dc} = 0$, and (a) $\beta = 1.27 \pm 0.01$; (b) $\beta = 1.27 \pm 0.05$; (c) $\beta = 1.27 \pm 0.1$. The corresponding curves for the same SQUID metamaterial without disorder are shown in black dotted lines.

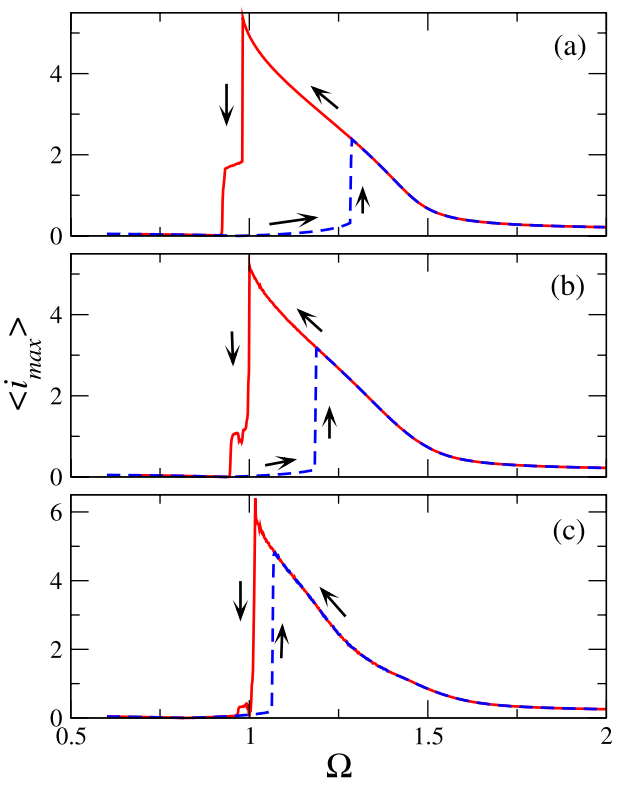

Figure 8. Current amplitude averaged over $n_R = 30$ realizations of disorder, $\langle i_{max} \rangle$, as a function of the driving frequency Ω for a SQUID metamaterial with $\alpha = 0.002$, $\beta = 0.15$, $\phi_{ac} = 0.02$, $\phi_{dc} = 0$, and (a) $\beta = 0.15 \pm 0.01$; (b) $\beta = 0.15 \pm 0.05$; (c) $\beta = 0.15 \pm 0.1$.

of the same SQUID metamaterials as before, taking into account the distribution of the parameters β of individual SQUIDs. To obtain reliable results, we have taken statistical averages over many realizations, n_R, of disorder. Remarkably, the calculations reveal that weak disorder strongly favors bistability, as observed in figures 7 and 8 for mean values of $\beta = 1.27$ and 0.15, respectively. In these figures, as we go from (a) to (c) β fluctuates by ± 0.01, ± 0.05, and ± 0.1, so that the relative disorder strength is much larger in figure 8. In all cases shown, either exhibiting weak or strong disorder, the stability of the nearly homogeneous states with high current amplitude increases considerably with respect to that for the corresponding ordered SQUID metamaterials. This is actually reflected in the widening of the bistability regions of the current amplitude–frequency curves. We should also note that the bistability region shrinks gradually with increasing strength of disorder. That shrinking occurs more rapidly for $\beta_L \simeq 1$ (figure 8) since the relative β variation is larger in this case.

4. Synchronization and multiresponse

In order to ensure that the current amplitude–frequency curves presented in figures 7 and 8 correspond to homogeneous states, we define and calculate a (Kuramoto-type) synchronization parameter, as

$$\Psi = \left\langle \frac{1}{N_x N_y} \sum_{n,m} e^{2\pi i \phi_{n,m}} \right\rangle_{\tau, n_R}, \qquad (22)$$

where the brackets denote averaging both in time (i.e., in one oscillation period) and the number of realizations of disorder n_R. The absolute value of Ψ quantifies the degree of synchronization; $|\Psi|$ may vary between 0 and 1, corresponding to completely asynchronous and synchronized states, respectively. The calculated values of $|\Psi|$ for (parts of) the current amplitude–frequency curves presented in figure 7 are shown in figure 9 for Ω varying in both directions. The bistability regions are shown in this figure as green dotted vertical lines, for reference. For very weak disorder (figure 9(a)), $|\Psi|$ remains close to unity for most of the frequency interval shown. However, there is a narrow region at low frequencies where synchronization, and therefore complete homogeneity breaks down, when the high current amplitude solution loses its stability. In that case all the SQUIDs change their state towards a lower current amplitude state. During the process, the phase differences of the SQUID fluxes and the driving field lock in randomly selected values, resulting in a low current amplitude and an only partially synchronized state. However, the two low current amplitude states that can be distinguish in this frequency region, i.e., the synchronized one obtained with increasing frequency and

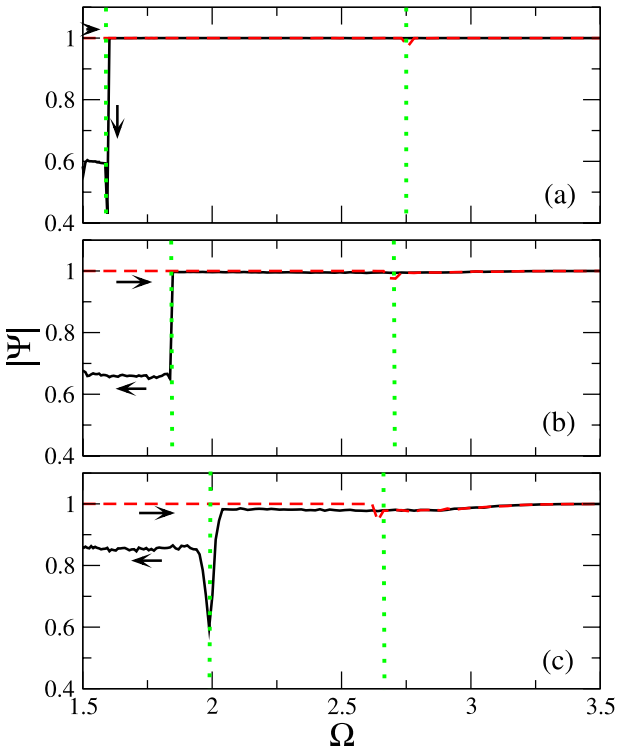

Figure 9. The magnitude of the synchronization parameter $|\Psi|$ as a function of the driving frequency Ω in the bistability region, for a $N_x \times N_y = 20 \times 20$ SQUID metamaterial with $\alpha = 0.002$, $\beta = 1.27 \pm 0.01$, $\phi_{ac} = 0.1$, $\phi_{dc} = 0$, $n_R = 30$ realizations of disorder, and (a) $\beta = 1.27 \pm 0.01$; (b) $\beta = 1.27 \pm 0.05$; $\beta = 1.27 \pm 0.1$. The arrows indicate the direction of frequency variation while the green dotted lines indicate the corresponding bistability intervals.

the partially synchronized one obtained with decreasing frequency, provide almost the same current amplitude. With increasing strength of the disorder (figure 9(b)) the bistability region shrinks while the same effect as in figure 9(a) is observed in a wider frequency interval. Moreover, the high current amplitude states are not completely synchronized in the bistability region, since $|\Psi|$ is slightly less than unity. The effect can be seen more clearly by further increasing the strength of the disorder as in figure 9(c), where $|\Psi|$ is clearly less than unity in the bistability region, indicating partial synchronization.

The magnetic response of the SQUID metamaterial at a particular state can be calculated in terms of the magnetization along the lines given in references [17, 23]. Assuming a tetragonal unit cell with $d_x = d_y = d$ and a squared SQUID area of side α, the magnetization is

$$M = \frac{\alpha^2 \langle I \rangle}{d^2 D}, \tag{23}$$

where $\langle I \rangle = I_c \langle i \rangle \equiv I_c \frac{1}{N_x N_y} \sum_{n,m} \langle i_{n,m} \rangle_\tau$ is the spatially and temporally averaged current, and D is a length related to the cavity where the metamaterial is placed [23]. Using fundamental relations of electromagnetism we write the relative magnetic permeability as

$$\mu_r = 1 + \frac{M}{H}, \tag{24}$$

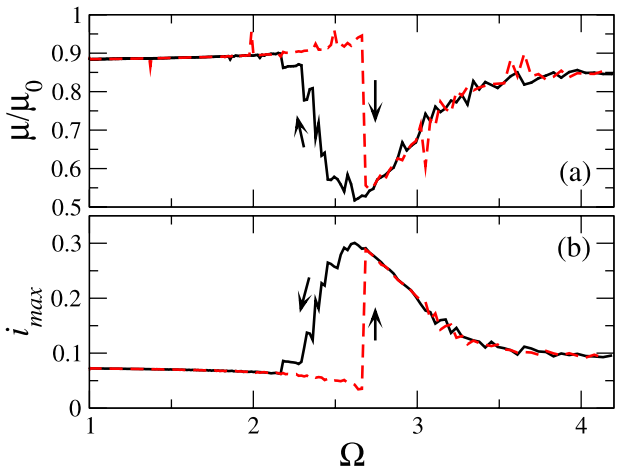

Figure 10. (a) Relative magnetic permeability $\mu_r = \mu/\mu_0$ for the low and high current amplitude states as a function of the driving frequency Ω, for $N_x = N_y = 20$, $\alpha = 0.002$, $\beta = 1.27$, $\phi_{ac} = 0.1$, and $\phi_{dc} = 0$. A multiple-valued magnetic response is observed in the bistability region. (b) The corresponding current amplitude–frequency curves. The arrows indicate the direction of frequency variation.

where H is the intensity of a spatially uniform magnetic field applied perpendicularly to the SQUID metamaterial plane. The latter is related to the external flux to the SQUIDs as

$$H = \frac{\Phi_0}{\mu_0 \alpha^2} \langle \phi_{ext} \rangle, \tag{25}$$

where μ_0 is the magnetic permeability of the vacuum, and the brackets denote temporal averaging. Combining equations (23)–(25), we get

$$\mu_r = 1 + \kappa \frac{\langle i \rangle}{\langle \phi_{ext} \rangle}, \tag{26}$$

where $\kappa = \frac{\mu_0 \alpha I_c}{\Phi_0} \frac{\alpha^3}{d^2 D}$. For a rough estimation of the constant κ we assume that $L \sim \mu_0 \alpha$, where L is the SQUID inductance, and that $D \simeq d$. Then, we have that $\kappa \sim \beta (\frac{\alpha}{d})^3$. Using $\alpha = d/2$ and $\beta = 1.27$ we get $\kappa \simeq 0.16$. We may then use the numerically calculated values of $i_{n,m}$ and ϕ_{ext} in equation (26) to obtain μ_r. Simultaneously stable SQUID metamaterial states respond differently to the external field and therefore exhibit different μ_r. This can be seen clearly in figure 10, where the relative permeability μ_r has been calculated from equation (26). The SQUID metamaterial for the parameters used in figure 10 is diamagnetic for all frequencies; however, the diamagnetic response is stronger for the high current states in the bistability region. For a weaker driving field that provides a flux amplitude of 10^{-3} the metamaterial is in the linear limit, as can be inferred by inspection of the current–frequency curve shown in figure 11(b). The corresponding μ_r as a function of the driving frequency Ω is again diamagnetic everywhere except close to the resonance, where strong variation of μ_r occurs. For frequencies below (but very close to) the single SQUID resonance ($\Omega_{SQ} \simeq 3$ for $\beta = 1.27$) the metamaterial becomes strongly paramagnetic. In contrast, for frequencies above (but very close to) the resonance the metamaterial becomes extremely diamagnetic,

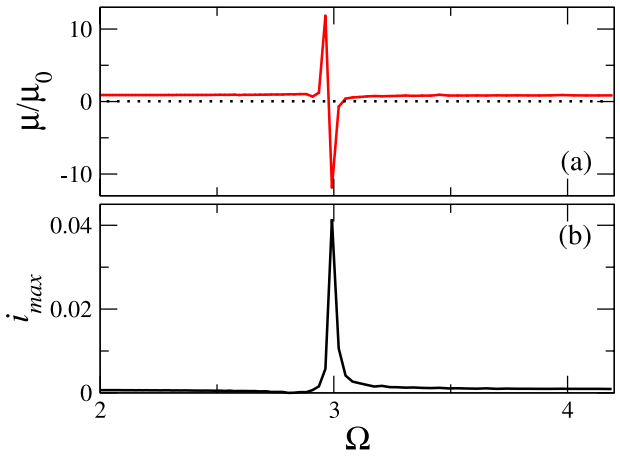

Figure 11. (a) Relative magnetic permeability $\mu_r = \mu/\mu_0$ for the low and high current amplitude states as a function of the driving frequency Ω, for $N_x = N_y = 20$, $\alpha = 0.002$, $\beta = 1.27$, $\phi_{ac} = 0.001$, and $\phi_{dc} = 0$. Negative μ_r is observed in a narrow frequency band just above the resonance frequency. (b) The corresponding current amplitude–frequency curves.

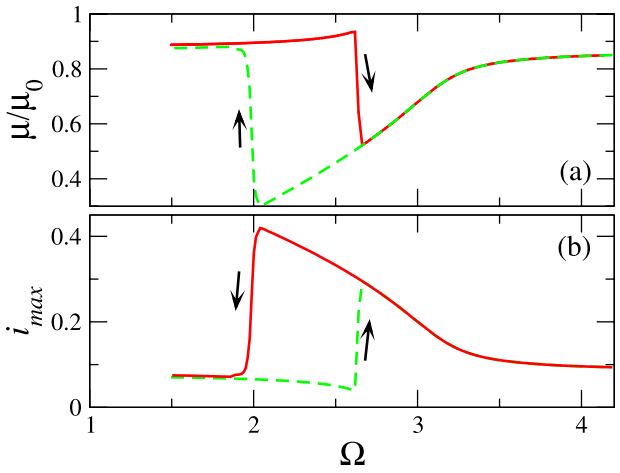

Figure 12. (a) Relative magnetic permeability $\mu_r = \mu/\mu_0$ for the low and high current amplitude states as a function of the driving frequency Ω, for a disordered SQUID metamaterial with $N_x = N_y = 20$, $\alpha = 0.002$, $\beta = 1.27 \pm 0.1$, $\phi_{ac} = 0.1$, and $\phi_{dc} = 0$. A multiple-valued magnetic response is observed in the bistability region. (b) The corresponding current amplitude–frequency curves.

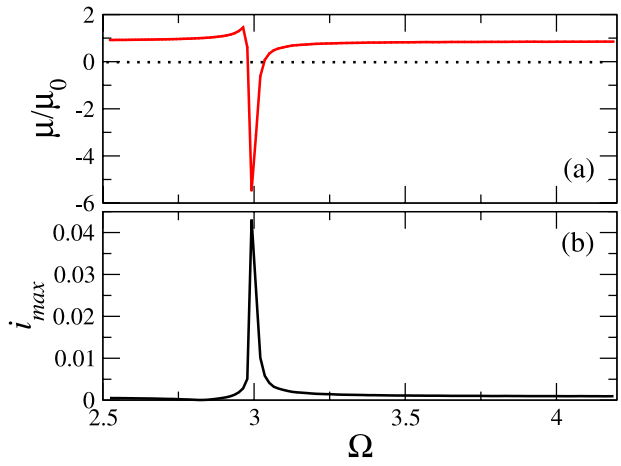

Figure 13. (a) Relative magnetic permeability $\mu_r = \mu/\mu_0$ for the low and high current amplitude states as a function of the driving frequency Ω, for a disordered SQUID metamaterial, with $N_x = N_y = 20$, $\alpha = 0.002$, $\beta = 1.27 \pm 0.01$, $\phi_{ac} = 0.001$, and $\phi_{dc} = 0$. Negative μ_r is observed in a narrow frequency band just above the resonance frequency. (b) The corresponding current amplitude–frequency curves.

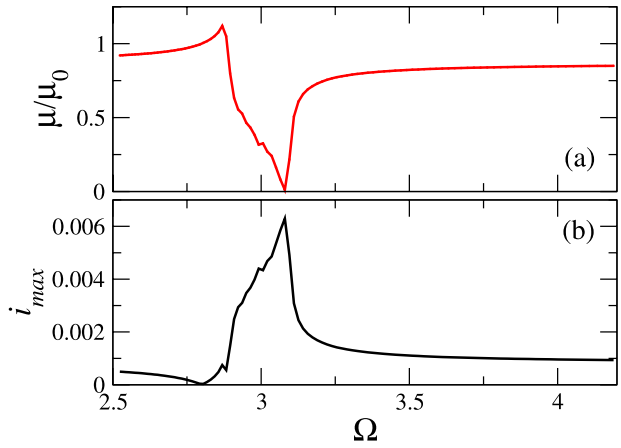

Figure 14. (a) Relative magnetic permeability $\mu_r = \mu/\mu_0$ for the low and high current amplitude states as a function of the driving frequency Ω, for a disordered SQUID metamaterial with $N_x = N_y = 20$, $\alpha = 0.002$, $\beta = 1.27 \pm 0.1$, $\phi_{ac} = 0.001$, and $\phi_{dc} = 0$. Negative μ_r is not observed because of the relatively strong disorder. (b) The corresponding current amplitude–frequency curves.

exhibiting negative μ_r within a narrow frequency region. Note that in this case negative μ_r would have also been obtained with a much smaller coefficient κ.

For a disordered SQUID metamaterial that is relatively strongly driven ($\phi_{ac} = 0.1$), the relative permeability μ_r changes only slightly. The most important effect observed in this case is the enlargement of the bistability interval (figure 12). For a weakly driven, disordered SQUID metamaterial, increasing disorder results in decreasing of the magnitude of μ_r in the frequency region around resonance. This effect is illustrated in figures 13 and 14, obtained for two different values of disorder; β fluctuates around its mean value by ± 0.01 and ± 0.1, respectively. In the frequency region around resonance, in particular, we observe in figure 13 that the dip corresponding to negative μ_r becomes shallower than that for the ordered SQUID metamaterial (figure 11). With further increasing disorder (figure 14), the negative μ_r region disappears. For this particular set of parameters, the minimum of μ_r touches the zero axis.

5. Conclusions

We have investigated numerically two-dimensional SQUID metamaterials driven by an alternating magnetic field. We have calculated current amplitude–frequency curves both for ordered and disordered metamaterials; in both cases we observed bistability regions created by almost homogeneous high and low current amplitude states. However, we observed that the presence of disorder widens significantly the

bistability regions. The effect is rather strong for SQUID metamaterials comprising SQUIDs with either a small or large β_L parameter. Remarkably, the homogeneity of high and low current amplitude states, which is quantified by the parameter Ψ, persists also in the case of disorder up to a very high degree. These states deviate only slightly from practically complete homogeneity only in the case of strong disorder, as can be seen from calculations of the amplitude of Ψ. This important result indicates that random variation of the SQUID parameters does not destroy bistability, which is crucial for applications that require bistable switching properties, but instead stabilizes the system against modulational or other instabilities. Bistability has actually been used in the past as a tool for quantum non-demolition measurements, where the read-out of a superconducting flux qubit is carried out by probing the hysteretic behavior of a coupled nonlinear resonator [65]. The SQUID metamaterial presented in this work could possibly be used in a similar way, replacing the nonlinear resonator.

This result is related to prior work on disordered networks of nonlinear oscillators, where it was concluded that moderate disorder may enhance synchronization and stabilize the system against chaos [66, 67]. Stabilization of Josephson circuits against chaos, in particular, has been recently demonstrated by numerical simulations in the time domain [68]. Moreover, the experimental demonstration of the stabilization of qubit spectral resonance with random pulses has been achieved [69]. In the present context, synchronization of individual SQUIDs in the high or low current amplitude states results in a high or low current amplitude for the metamaterial. This requires that (almost) all SQUIDs are in phase. It could be natural to assume that the more nearly identical the elements, the better the synchronization will be. However, even in the ideal case of identical elements, the earlier assumption may not be true and the in-phase state may be dynamically unstable. Then, synchronization is reduced and the SQUID metamaterial cannot remain in the high current amplitude state, which is more sensitive to instability. This can be clearly observed in figures 5(b) and 6(b), where in most of the bistability region the metamaterial relaxes to partially synchronized states that provide significantly lower current amplitude. This type of disorder-assisted self-organization may also occur by introducing local disorder in an array of otherwise identical oscillators, i.e., in the form of impurities [70, 71]. In this case, the impurities trigger a self-organizing process that brings the system to complete synchronization and suppression of chaotic behavior.

Having calculated numerically the response of the metamaterial to an alternating field with given frequency, we have calculated the magnetic permeability of the metamaterial for several illustrating cases both with and without disorder. While the expression for calculating the magnetic permeability is rather simple, there is some uncertainty about the value of the factor κ. However, for a reasonable value of κ we observe that the magnetic permeability can take negative values in a narrow frequency region above resonance for weakly driven SQUID metamaterials. In this case, increasing disorder results in weakening the negative response of the metamaterial; thus, for relatively strong disorder the response is not sufficient to make the magnetic permeability negative. For SQUID metamaterials exhibiting bistability, different magnetic permeabilities can be reached under the same conditions, depending on their state.

Acknowledgments

This research was partially supported by the THALES Project MACOMSYS, co-financed by the European Union (European Social Fund ESF) and Greek national funds through the Operational Program 'Education and Lifelong Learning' of the National Strategic Reference Framework (NSRF)—Research Funding Program: THALES. Investing in knowledge society through the European Social Fund.

References

[1] Shalaev V M 2007 Optical negative-index metamaterials *Nature Photon.* **1** 41–8
[2] Soukoulis C M, Linden S and Wegener M 2007 Negative refractive index at optical wavelengths *Science* **315** 47–9
[3] Litchinitser N M and Shalaev V M 2008 Photonic metamaterials *Laser Phys. Lett.* **5** 411–20
[4] Zheludev N I 2010 The road ahead for metamaterials *Science* **328** 582–3
[5] Pendry J B 2000 Negative refraction makes a perfect lens *Phys. Rev. Lett.* **85** 3966–9
[6] Schurig D, Mock J J, Justice B J, Cummer S A, Pendry J B, Starr A F and Smith D R 2006 Metamaterial electromagnetic cloak at microwave frequencies *Science* **314** 977–80
[7] Zheludev N I 2011 A roadmap for metamaterials *Opt. Photon. News* **22** 31–5
[8] Caputo J-G, Gabitov I and Maimistov A I 2012 Electrodynamics of a split-ring Josephson resonator in a microwave line *Phys. Rev.* B **85** 205446
[9] Shadrivov I V, Kozyrev A B, van der Weide D W and Kivshar Yu S 2008 Tunable transmission and harmonic generation in nonlinear metamaterials *Appl. Phys. Lett.* **93** 161903
[10] Boardman A D, Grimalsky V V, Kivshar Y S, Koshevaya S V, Lapine M, Litchinitser N M, Malnev V N, Noginov M, Rapoport Y G and Shalaev V M 2010 Active and tunable metamaterials *Laser Photon. Rev.* **5** 287–307
[11] Anlage S M 2011 The physics and applications of superconducting metamaterials *J. Opt.* **13** 024001
[12] Ricci M C, Orloff N and Anlage S M 2005 Superconducting metamaterials *Appl. Phys. Lett.* **87** 034102
[13] Ricci M C, Xu H, Prozorov R, Zhuravel A P, Ustinov A V and Anlage S M 2007 Tunability of superconducting metamaterials *IEEE Trans. Appl. Supercond.* **17** 918–21
[14] Gu J, Singh R, Tian Z, Cao W, Xing Q, He M -X, Zhang J W, Han J, Chen H and Zhang W 2010 Terahertz superconductor metamaterial *Appl. Phys. Lett.* **97** 071102
[15] Fedotov V A, Tsiatmas A, Shi J H, Buckingham R, de Groot P, Chen Y, Wang S and Zheludev N I 2010 Temperature control of Fano resonances and transmission in superconducting metamaterials *Opt. Express* **18** 9015–9
[16] Chen H-T, Yang H, Singh R, O'Hara J F, Azad A K, Stuart A, Trugman S A, Jia Q X and Taylor A J 2010 Tuning the resonance in high-temperature superconducting terahertz metamaterials *Phys. Rev. Lett.* **105** 247402

[17] Lazarides N and Tsironis G P 2007 rf superconducting quantum interference device metamaterials *Appl. Phys. Lett.* **16** 163501
[18] Lazarides N, Tsironis G P and Eleftheriou M 2008 Dissipative discrete breathers in rf SQUID metamaterials *Nonlinear Phenom. Complex Syst.* **11** 250–8
[19] Barone A and Patternó G 1982 *Physics and Applications of the Josephson Effect* (New York: Wiley)
[20] Likharev K K 1986 *Dynamics of Josephson Junctions and Circuits* (Philadelphia, PA: Gordon and Breach)
[21] Tsironis G P, Lazarides N and Eleftheriou M 2009 Dissipative breathers in rf SQUID metamaterials *PIERS Online* **5** 26–30
[22] Lazarides N and Tsironis G P 2012 Intrinsic localization in nonlinear and superconducting metamaterials *Proc. SPIE* **8423** 84231K
[23] Jung P, Butz S, Shitov S V and Ustinov A V 2013 Low-loss tunable metamaterials using superconducting circuits with Josephson junctions *Appl. Phys. Lett.* **102** 062601
[24] Butz S, Jung P, Filippenko L V, Koshelets V P and Ustinov A V 2013 A one-dimensional tunable magnetic metamaterial arXiv:1304.7371 [cond-mat.supr-con]
[25] Butz S, Jung P, Filippenko L V, Koshelets V P and Ustinov A V 2013 Protecting SQUID metamaterials against stray magnetic field arXiv:1305.2910 [cond-mat.supr-con]
[26] Kleiner R, Koelle D, Ludwig F and Clarke J 2004 Superconducting quantum interference devices: State of the art and applications *Proc. IEEE* **92** 1534–48
[27] Fagaly R L 2006 Superconducting quantum interference device instruments and applications *Rev. Sci. Instrum.* **77** 101101
[28] Wernsdorfer W 2009 From micro- to nano-SQUIDs: applications to nanomagnetism *Supercond. Sci. Technol.* **22** 064013
[29] Beyer J and Drung D 2008 A SQUID series array dc current sensor *Supercond. Sci. Technol.* **21** 095012
[30] Häussler Ch, Träuble T, Oppenländer J and Schopohl N 2001 LC-resonant voltage response of superconducting quantum interference filters *IEEE Trans. Appl. Supercond.* **11** 1275–8
[31] Bruno A C and Espy M A 2004 Design of a SQUID array as a discrete spatial filter *Supercond. Sci. Technol.* **17** 908–15
[32] Matsuda M, Nakamura K, Mikami H and Kuriki S 2005 Fabrication of magnetometers with multiple-SQUID arrays *IEEE Trans. Appl. Supercond.* **15** 817–20
[33] Hirayama F, Kasai N and Koyanagi M 1999 Design of series SQUID array suppressing Josephson oscillation interference between element-squiss *IEEE Trans. Appl. Supercond.* **9** 2923–6
[34] Huber M E, Neil P A, Benson R G, Burns D A, Corey A M, Flynn C S, Kitaygorodskaya Y, Massihzadeh O, Martinis J M and Hilton G C 2001 DC SQUID series array amplifiers with 120 MHz bandwidth *IEEE Trans. Appl. Supercond.* **11** 1251–6
[35] Castellanos-Beltran M A and Lehnert K W 2007 Widely tunable parametric amplifier based on a superconducting quantum interference device array resonator *Appl. Phys. Lett.* **91** 083509
[36] Kaplunenko V K, Mygind J, Pedersen N F and Ustinov A V 1993 Radiation detection from phase-locked serial dc SQUID arrays *J. Appl. Phys.* **73** 2019–23
[37] Häussler Ch, Oppenländer J and Schopohl N 2001 Nonperiodic flux to voltage conversion of series array of dc superconducting quantum interference devices *J. Appl. Phys.* **89** 1875–9
[38] Kornev V K, Soloviev I I, Klenov N V, Sharafiev A V and Mukhanov O A 2012 Array designs for active electrically small superconductive antennas *Physica* C **479** 119–22
[39] Kornev V K, Soloviev I I, Sharafiev A V, Klenov N V and Mukhanov O A 2013 Active electrically small antenna based on superconducting quantum array *IEEE Trans. Appl. Supercond.* **23** 1800405
[40] Snigirev O V, Chukharkin M L, Kalabukhov A S, Tarasov M A, Deleniv A A, Mukhanov O A and Winkler D 2007 Superconducting quantum interference filters as rf amplifiers *IEEE Trans. Appl. Supercond.* **17** 718–21
[41] Kornev V K, Soloviev I I, Klenov N V and Mukhanov O A 2009 High-linearity SQIF-like Josephson junction structures *IEEE Trans. Appl. Supercond.* **19** 741–4
[42] Kornev V K, Soloviev I I, Klenov N V and Mukhanov O A 2007 Development of SQIF-based output broad band amplifier *IEEE Trans. Appl. Supercond.* **17** 569–72
[43] Mukhanov O A, Rylov S R, Gaidarenko D V, Dubash N B and Borzenets V V 1997 Josephson output interfaces for rsfq circuits *IEEE Trans. Appl. Supercond.* **7** 2826–31
[44] Mukhanov O A, Inamdar A, Pilippov T, Sahu A, Sarwana S and Semenov V 2007 Superconductor components for direct digital synthesizer *IEEE Trans. Appl. Supercond.* **17** 416–21
[45] Brandel O, Wetzstein O, May T, Toepfer H, Ortlepp T and Meyer H -G 2012 Rsfq electronics for controlling superconducting polarity switches *Supercond. Sci. Technol.* **25** 125012
[46] Poletto S, Chiarello F, Castellano M G, Lisenfeld J, Lukashenko A, Carelli P and Ustinov A V 2009 A tunable rf SQUID manipulated as flux and phase qubits *Physica Scr.* **T137** 014011
[47] Castellano M G, Chiarello F, Carelli P, Cosmelli C, Mattioli F and Torrioli G 2010 Deep-well ultrafast manipulation of a SQUID flux qubit *New J. Phys.* **12** 043047
[48] Zhou Z, Chu S-I and Han S 2005 Quantum entanglement and controlled logical gates using coupled SQUID flux qubits *IEEE Trans. Appl. Supercond.* **15** 833–6
[49] Roscilde T, Corato V, Ruggiero B and Silvestrini P 2005 A multi-qubit system for a scalable adiabatic quantum evolution *Phys. Lett.* A **345** 224–30
[50] Johnson M W *et al* 2010 A scalable control system for a superconducting adiabatic quantum optimization processor *Supercond. Sci. Technol.* **23** 065004
[51] Castellanos-Beltran M A, Irwin K D, Hilton G C, Vale L R and Lehnert K W 2008 Amplification and squeezing of quantum noise with a tunable Josephson metamaterial *Nature Phys.* **4** 928–31
[52] Risté D, Bultink C C, Lehnert K W and DiCarlo L 2012 Feedback control of a solid-state qubit using high-fidelity projective measurement *Phys. Rev. Lett.* **109** 240502
[53] Lähteenmäki P, Paraoanu G S, Hassel J and Hakonen P J 2013 Dynamical casimir effect in a Josephson metamaterial *Proc. Natl. Acad. Sci.* **110** 4234–8
[54] Teufel J D, Donner T, Castellanos-Beltran M A, Harlow J W and Lehnert K W 2009 Nanomechanical motion measured with an imprecision below that at the standard quantum limit *Nature Nanotechnol.* **4** 820–3
[55] Roch N, Flurin E, Nguyen F, Morfin P, Campagne-Ibarcq P, Devoret M H and Huard B 2012 Widely tunable, nondegenerate three-wave mixing microwave device operating near the quantum limit *Phys. Rev. Lett.* **108** 147701
[56] Josephson B 1962 Possible new effects in superconductive tunnelling *Phys. Lett.* A **1** 251–5
[57] Shnyrkov V I, Khlus V A and Choi G M 1980 On quantum interference in a superconducting ring closed by a weak link *J. Low Temp. Phys.* **39** 477–96
[58] Zeng X H, Zhang Y, Chesca B, Barthel K, Greenberg Ya S and Braginski A I 2000 Experimental study of amplitude–frequency characteristics of high-transition-temperature radio frequency superconducting quantum interference devices *J. Appl. Phys.* **88** 6781–7

[59] Palacios-Laloy A, Nguyen F, Mallet F, Bertet P, Vion D and Esteve D 2008 Tunable resonators for quantum circuits *J. Low Temp. Phys.* **151** 1034–42
[60] Kourakis I, Lazarides N and Tsironis G P 2007 Self-focusing and envelope pulse generation in nonlinear magnetic metamaterials *Phys. Rev.* E **75** 067601
[61] Shamonina E, Kalinin V A, Ringhofer K H and Solymar L 2002 Magneto-inductive waves in 1-, 2- and 3-dimensions *J. Appl. Phys.* **92** 6252–61
[62] Berggren S *et al* 2013 Development of 2d bi-SQUID arrays with high linearity *IEEE Trans. Appl. Supercond.* **23** 1400208
[63] Prokopenko G V, Mukhanov O A, Leese de Escobar A, Taylor B, de Andrade M C, Berggren S, Longhini P, Palacios A, Nisenoff M and Fagaly R L 2013 DC and rf measurements of serial bi-SQUID arrays *IEEE Trans. Appl. Supercond.* **23** 1400607
[64] Longhini P *et al* 2012 Voltage response of non-uniform arrays of bi-superconductive quantum interference devices *J. Appl. Phys.* **111** 093920
[65] Lupascu A, Saito S, Picot T, de Groot P C, Harmans C J P M and Mooij J E 2007 Quantum non-demolition measurement of a superconducting two-level system *Nature Phys.* **3** 119
[66] Braiman Y, Ditto W L, Wiesenfeld K and Spano M L 1995 Disordered-enhanced synchronization *Phys. Lett.* A **206** 54–60
[67] Braiman Y, Lindner J F and Ditto W L 1995 Taming spatiotemporal chaos with disorder *Nature* **378** 465–7
[68] Gustavsson S, Bylander J and Oliver W D 2013 Time-reversal symmetry and universal conductance fluctuations in a driven two-level system *Phys. Rev. Lett.* **110** 016603
[69] Li Jian *et al* 2013 Motional averaging in a superconducting qubit *Nat. Comms.* **4** 1420
[70] Gavrielides A, Kottos T, Kovanis V and Tsironis G P 1998 Self-organization of coupled nonlinear oscillators through impurities *Europhys. Lett.* **44** 559–64
[71] Gavrielides A, Kottos T, Kovanis V and Tsironis G P 1998 Spatiotemporal organization of coupled nonlinear pendula through impurities *Phys. Rev.* E **58** 5529–34